ADVANCED MATERIALS

Supporting Information

for *Adv. Mater.*, DOI 10.1002/adma.202402981

Customized Enhancement of Thermal Sensitivity of Tumors at Different Subcutaneous Depths by Multichannel Lanthanide Nanocomposites

Yuxin Liu, Zheng Wei, Jieying Zhang, Yang Xu, Jing Zhou, Zhanfang Ma, Francesco G. Mutti, Hong Zhang, Xingjun Zhu* and Felix F. Loeffler**

Supplementary information

Customized enhancement of thermal sensitivity of tumors at different subcutaneous depths by multichannel lanthanide nanocomposites

Yuxin Liu[1,3,5], Zheng Wei[3], Jieying Zhang[2], Yang Xu[4], Prof. Dr. Jing Zhou[4], Prof. Dr. Zhanfang Ma[4], Prof. Dr. Francesco G. Mutti[3], Prof. Dr. Hong Zhang*[3], Dr. Xingjun Zhu*[2], and Dr. Felix F. Loeffler*[1]

1. Department of Biomolecular Systems, Max-Planck Institute of Colloids and Interfaces, 14476 Potsdam (Germany). E-mail: Felix.Loeffler@mpikg.mpg.de
2. School of Physical Science and Technology, Shanghai Tech University, 201210 Shanghai (China). E-mail: zhuxj1@shanghaitech.edu.cn
3. Van' t Hoff Institute for Molecular Sciences, Molecular Photonics & HIMS-Biocat University of Amsterdam, 1098 XH Amsterdam (The Netherlands). E-mail: H.Zhang@uva.nl
4. Beijing Key Laboratory for Optical Materials and Photonic Devices, Capital Normal University, Beijing 100048 (China).
5. Institute of Chemistry and Biochemistry, Free University of Berlin, 14195 Berlin (Germany).

Materials and Methods

Materials: Lanthanide oxide $LuCl_3$ (99.999%), $YbCl_3$ (99.999%) and $TmCl_3$ (99.99%), 1-octadecene (ODE), and NH_4F were purchased from Alfa Aesar Chemical Co. Ltd. Other chemicals were purchased from Sigma Aldrich. All bioreagents for cell culture and others were provided by Life Technologies Co., Ltd. All chemical reagents were of analytical grade and were used directly without further purification. Deionized (DI) water was used throughout.

Synthesis of $NaLuF_4$:Yb,Er,Tm: The uniform $NaLuF_4$:Yb,Er,Tm nanophosphor was synthesized by an optimized solvothermal method.(*1*) In a typical experiment, a mixture of 1 mmol $LnCl_3$ (Ln: 80%Lu, 18%Yb, 1%Er, and 1%Tm), 15 mL oleic acid (OA), and 15 mL ODE were added into a 100 mL three-necked flask. Under vacuum, the mixture was heated to 160 °C to form a clear solution, and then cooled to room temperature. After the solution had cooled down, 2.5 mmol NaOH (0.1 g) and 4 mmol NH_4F (0.1481 g) were added into the flask directly and stirred for 30 minutes. The solution was slowly heated under gentle stirring, degassed at 100 °C, and then heated to 300 °C and maintained for 45 min under Argon atmosphere. After the solution had cooled down to room temperature (rt), the $NaLuF_4$:Yb,Er,Tm nanoparticles were separated *via* centrifugation (11180 × g) and washed with ethanol/cyclohexane (1:1 v/v) three times. The product was stored at rt in cyclohexane.

Synthesis of $NaLuF_4$:Yb,Er,Tm@$NaLuF_4$: Coating by a $NaLuF_4$ shell was performed by an optimized solvothermal procedure.(*2*) In a typical experiment, a mixture of 1 mM $LuCl_3$, 15 mL OA, and 15 mL ODE were added into a 100 mL three-necked flask. Under vacuum, the mixture was heated to 160 °C to form a clear solution, and then cooled to rt. After the solution cooled down, 0.025 mmol NaOH (0.1 g), 0.04 mmol NH_4F (0.1481 g), and as-prepared $NaLuF_4$:Yb,Er,Tm nanoparticles were added into the flask directly and stirred for 30 minutes. The solution was slowly heated under gentle stirring, degassed at 100 °C, and then heated to 300 °C and maintained for 1 hour under Argon atmosphere. After the solution cooled to rt, the $NaLuF_4$:Yb,Er,Tm@$NaLuF_4$ were separated *via* centrifugation (11180 × g) and washed with ethanol/cyclohexane (1:1 v/v) three times. The product was stored at rt in cyclohexane.

Synthesis of Ln-ZIF⊂rPMo, Ln-ZIF, and Ln-ZIF-PEG: The ZIF⊂rPMo shell was coated by a previously reported method with modification.(*3*) In a typical experiment, the rPMo was obtained by reducing commercial phosphomolybdic acid with excessive ascorbic acid, washed with acetone to purify, and dissolved in water for further use. 15 mL of $CHCl_3$ containing 1 g polyvinylpyrrolidone (PVP, Mw = 40,000) was mixed with 10 mL of trichloromethane ($CHCl_3$) containing 10 mg as-prepared $NaLuF_4$:Yb,Er,Tm@$NaLuF_4$ under stirring for 24 hours at 40 °C. After removing $CHCl_3$ by ethanol washing, Ln-PVP was dispersed in 10 mL of methanol. Then, 2 mL of the above-mentioned Ln-PVP dispersion, 10 mL of 2-methylimidazole solution (25

mM), 10 mL of $Zn(NO_3)_2 \cdot 6H_2O$ solution (25 mM), and 1 mL of rPMo solution (10 mg mL^{-1}) were mixed and then stirred for 24 hours at rt. The Ln-ZIF⊂rPMo were separated *via* centrifugation (11180 × g) and washed with ethanol and DI water. The final product was stored at 4 °C in saline buffer. The Ln-ZIF was obtained with a similar protocol without the addition of rPMo solution. The Ln-ZIF-PEG was prepared by a typical PEGylation protocol. In a typical experiment, 10 mL of Ln-ZIF dispersion (1 mg mL^{-1}) was mixed with 10 mL of PEG solution (1 mg mL^{-1}) and stirred overnight at rt. The Ln-ZIF-PEG was then separated *via* centrifugation (11180 × g) and washed with DI water. The final product was stored at 4 °C in saline buffer.

EGCG loading experiment: In a typical experiment, 20 mg of studied material (Ln-ZIF⊂rPMo, Ln-ZIF, or Ln-ZIF-PEG) was dispersed in 10 mL DI water. Then, 5 mL aqueous solution containing the desired concentration of epigallocatechin gallate (EGCG) was added into the material dispersion. After 24 hours of gentle stirring at 4 °C, the EGCG-loaded material was separated *via* centrifugation (11180 × g) and washed with DI water for several times and stored at 4 °C in saline buffer.

Computational details: The crystal model was constructed with rPMo clusters uniformly distributed in ZIF-8 pores. The entire crystal model is constructed by repeating the pores; the classical molecular dynamics method optimizes the stable configuration. The absorption ability and water diffusion efficiency of ZIF-8 and ZIF⊂rPMo were simulated by utilizing the Sorption and Forcite package in Materials Studio, BIOVIA, US. The calculation was performed using grand canonical Monte Carlo (GCMC) simulations to compute the average number of adsorbed water molecules per unit cell of the material, with 1×10^6 steps for both equilibration run and data collection. A force field was used to describe van der Waals parameters, atomic bond radii, bond angles, and dihedral angles in all calculations.(*4*) The adsorption capacity was evaluated in terms of excess adsorption, which was defined as the number of additional water molecules stored in a given volume when adsorbing substrate is present, compared to free volume storage.(*5*) The Nosé–Hoover chain constant temperature algorithm was applied to control the diffusion of water molecules in the materials at the temperature of 298 K.(*6*) Velocity-Verlet quaternions were used to integrate the position and speed with a time step of 1 fs and a cutoff distance of Lennard-Jones and Coulomb interaction of 12 Å.(*7*)

Calculation of fluorescent thermometer parameters: The thermal sensitivity of Ln-ZIF⊂rPMo was calculated by a standard equation for ratiometric fluorescent nanothermometers (*8*):

$$S = \frac{1}{R}\frac{dR}{dT}, \qquad \text{(Equation S1)}$$

where S is the thermal sensitivity, R is the I_{525}/I_{545} fluorescence ratio, and T is the temperature in Kelvin. The temperature uncertainty of Ln-ZIF⊂rPMo was calculated by an equation in first order approximation:

$$\delta T = \frac{1}{S}\frac{\Delta I}{I}, \qquad \text{(Equation S2)}$$

where δT is the temperature uncertainty, S is the thermal sensitivity, ΔI is the background noise of the

fluorescence spectrum and I is the fluorescence intensity.

Characterization: The sizes and morphologies of $NaLuF_4$:Yb,Er,Tm, $NaLuF_4$: Yb,Er,Tm@$NaLuF_4$, Ln-ZIF, and Ln-ZIF⊂rPMo were determined using an FEI Tecnai G^2F30 transmission electron microscope (TEM). Samples of the above nanoparticles were deposited on the surface of a copper grid. Energy-dispersive X-ray analysis line scan and scanning transmission electron microscopy (STEM) of the samples were also performed during TEM measurements. UV-vis-NIR absorption and transmittance spectra were obtained on a Shimadzu UV-3600 UV-vis-NIR spectrophotometer. The fluorescence spectra were taken on a FLS980 lifetime and steady state spectrometer (Edinburgh Instruments). Photothermal temperature curves and thermal images were determined by a temperature determination system equipped with a thermocouple thermometer and a NIR camera (FLIR E40). ζ potential experiments are carried out on an ALV-5000 spectrometer goniometry equipped with an ALV/LSE-5004 light scattering electronic and multiple tau digital correlator and a JDS Uniphase He–Ne laser (632.8 nm) with an output power of 22 mW.

Cell culture and MTT assays: Mouse breast cancer cell lines (4T1 cell line) were provided by the Institute of Basic Medical Sciences, Chinese Academy of Medical Sciences. Cells were grown in DMEM (Dulbecco's Modified Eagle's medium), supplemented with 10% FBS (fetal bovine serum) and 1% penicillin-streptomycin at 37 °C with 5% CO_2. Cultures were maintained at 37 °C under a humidified atmosphere containing 5% CO_2. The cultured 4T1 cells (90 μL $well^{-1}$, 10^5 cells mL^{-1}) were seeded into a 96-well cell culture plate, and the cells were incubated at 37 °C under 5% CO_2 for 24 h. Medium of Ln-ZIF⊂rPMo-EGCG (10 μL $well^{-1}$, containing 1% PBS) and medium containing 1% PBS (10 μL $well^{-1}$) was set as a control group. The cells received different irradiation prescriptions under different tissue coverage, and then incubated at 37 °C under 5% CO_2 for 24 h, respectively. Subsequently, 3-(4,5-dimethylthiazol-2-yl)-2,5-diphenyltetrazolium bromide (MTT, 10 μL, 5 mg mL^{-1}) was added to each well of the 96-well plate and incubated for an additional 4 h. After addition of dimethyl sulfoxide (DMSO, 100 μL $well^{-1}$), the assay plate was allowed to stand at room temperature for 30 min. A Tecan Infinite M200 monochromator-based multifunction microplate reader was used to measure the OD570 (*Abs* value) of each well with background subtraction at 570 nm. A well without MTT was used as blank control. The following formula was used to calculate the viability of cell growth: Cell viability (100%) = (mean of *Abs.* value of treatment group - mean of *Abs.* value of blank)/mean *Abs.* value of control × 100%.

Hematology studies. All animal procedures were performed in accordance with the Guidelines for Care and Use of Laboratory Animals of Beijing Vital River Laboratory Animal Technology Co., Ltd. and approved by the Animal Ethics Committee of the Vital River Institutional Animal Care and Use Committee. Blood samples were harvested from mice intravenously injected with Ln-ZIF⊂rPMo-EGCG (n = 3, dose = 20 mg kg^{-1}, Test) and from mice receiving no injection, 1 day, 7 days, 15 days, 30 days, and 60 days post-injection (n = 3, dose = 0 mg kg^{-1}, Control), respectively. The body weight of the mice was also recorded. Blood was collected from

the femoral vein. Five important hepatic indicators (ALT, alanine aminotransferase; AST, aspartate amino transferase; TBIL, total bilirubin; ALB, albumin; TP, total protein) and one indicator for kidney functions (CREA, creatinine) were measured. Blood smears were prepared by placing a drop of blood on one end of a slide, and using another slide to disperse the blood along the length of the slide. The tissues (~1 cm × 1 cm) were harvested from the back and abdomen area of these mice after euthanasia, and used as soon as possible. Tissues were not frozen before use and used randomly without numbering.

Customized sensitization and therapy in vivo. The orthotopic tumor-bearing mouse model was established according to our previous work and treatment was performed when both tumor volumes reached ~60 mm^3. For customized sensitization and photothermal therapy, ten mice received intratumoral injection of Ln-ZIF⊂rPMo-EGCG (10 μL, 500 μg mL^{-1}). The right tumors were randomly covered with 0.5 – 1.5 mm of tissue, while the left ones remained bare. Tissue coverage and therapy were performed separately by two different operators to ensure reliability of this double-blind experiment: the selection of tissue thickness covering the tumors was decided by the first operator independently, without notifying the second one of the selections before performing therapeutic experiments. Therefore, the covered tissue thickness was random to the second operator. For tissue section staining, the tumors covered by 1.5 mm tissue were identified by the first operator. 60 min post-injection, the fluorescence signal was determined for each of the mice and, on the basis of calibration diagrams established in cell experiment, customized irradiation prescriptions were established for each tumor in the mice (*Abbr.* customized irradiation group). Within the therapeutic process, mice were anesthetized and received whole-body irradiation by using the ring-shape laser array (Figure S11).(*9*) The non-uniform light field for synergistic treatment was generated by a laser array containing 8 laser fibers, connected to an 8-channel laser (808 nm, output power 0-8 W). The positions of the laser fibers were fixed (holders not shown in the image), but the angle of fibers, size of laser spots, and output power could be independently modulated. The power density was quantified by a power meter. For fluorescence imaging and establishment of irradiation prescription, an Si-based and an InGaAs CCD were attached, while the 808 nm 8-channel laser was replaced by a 980 nm 8-channel laser. During the treatment, the mice were fixed on the stage with tape. In a typical experiment, it was sufficient to expand the laser spot size coming from one laser channel to irradiate one whole tumor, applying the required irradiation prescription derived from the data presented in Figures 3 and 4. The tumor sizes were measured by a caliper after treatment and calculated according to the formula: Tumor volume = (tumor length) × $(\text{tumor width})^2/2$. Two groups with same composition of mice and Ln-ZIF⊂rPMo-EGCG administration, irradiated by high laser power (1.25 W cm^{-2}, 180 s, *Abbr.* high irradiation group) or by low laser power (0.50 W cm^{-2}, 180 s, *Abbr.* low irradiation group), served as control groups.

1. Y. X. Liu *et al.*, Optimization of Prussian Blue Coated NaDyF4:x%Lu Nanocomposites for Multifunctional Imaging-Guided Photothermal Therapy. *Adv. Funct. Mater.* **26**, 5120-5130 (2016).
2. Y. X. Liu *et al.*, Rationally designed pure-inorganic upconversion nanoprobes for ultra-highly selective hydrogen sulfide imaging and elimination in vivo. *Chem. Sci.* **10**, 1193-1200 (2019).
3. Y. Jiang *et al.*, Near-infrared light-triggered NO release for spinal cord injury repair. *Sci. Adv.* **6**, eabc3513 (2020).
4. A. K. Rappe, C. J. Casewit, K. S. Colwell, W. A. Goddard, III, W. M. Skiff, UFF, a full periodic table force field for molecular mechanics and molecular dynamics simulations. *J. Am. Chem. Soc.* **114**, 10024-10035 (1992).
5. M. M. Biswas, T. Cagin, Simulation Studies on Hydrogen Sorption and Its Thermodynamics in Covalently Linked Carbon Nanotube Scaffold. *J. Phys. Chem. B* **114**, 13752-13763 (2010).
6. S. Labík, W. R. Smith, Scaled Particle Theory and the Efficient Calculation of the Chemical Potential of Hard Spheres in the NVT Ensemble. *Mol. Simul.* **12**, 23-31 (1994).
7. N. S. Martys, R. D. Mountain, Velocity Verlet algorithm for dissipative-particle-dynamics-based models of suspensions. *Phys. Rev. E* **59**, 3733-3736 (1999).
8. B. del Rosal *et al.*, Infrared-Emitting QDs for Thermal Therapy with Real-Time Subcutaneous Temperature Feedback. *Adv. Funct. Mater.* **26**, 6060-6068 (2016).
9. Y. Liu *et al.*, Multi-Channel Lanthanide Nanocomposites for Customized Synergistic Treatment of Orthotopic Multi-Tumor Cases. *Angew. Chem. Int. Ed.*, e202303570 (2023).

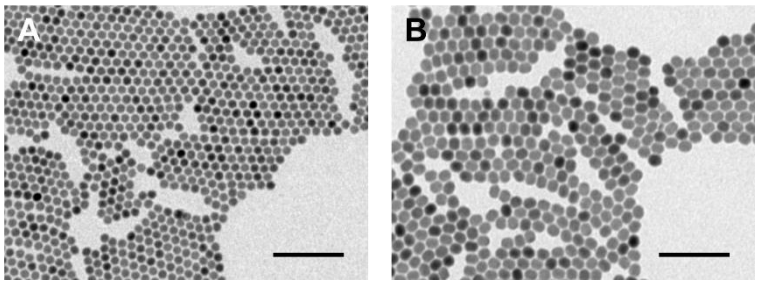

Figure S1. TEM images of $NaLuF_4$:Yb,Er,Tm (A) and $NaLuF_4$: Yb,Er,Tm@$NaLuF_4$ (B). Scale bar 100 nm.

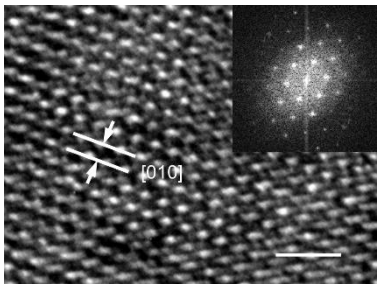

Figure S2. High-resolution TEM images of Ln-ZIF⊂rPMo. Scale bar 2 nm. Fast Fourier transformed (FFT) image was inserted.

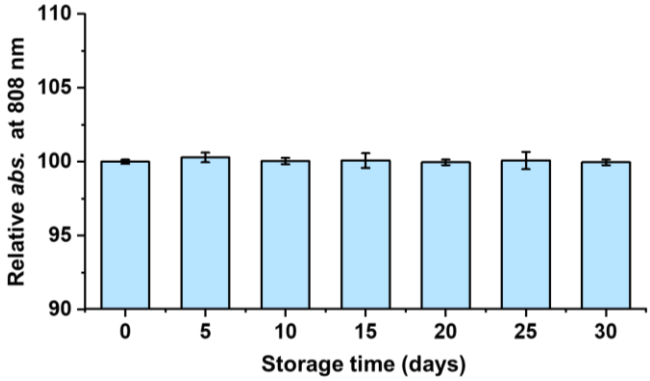

Figure S3. Relative absorbance of Ln-ZIF⊂rPMo at 808 nm after different days of storage. Data are represented as mean ± SD (n = 3).

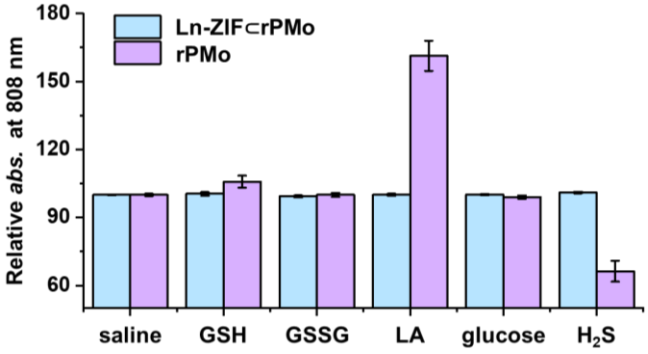

Figure S4. Relative absorbance of Ln-ZIF⊂rPMo and rPMo at 808 nm in the presence of various typical biomolecules in tumor microenvironment. GSH: reduced glutathione; GSSG: oxidized glutathione; LA: lactic acid. Data are represented as mean ± SD (n = 3).

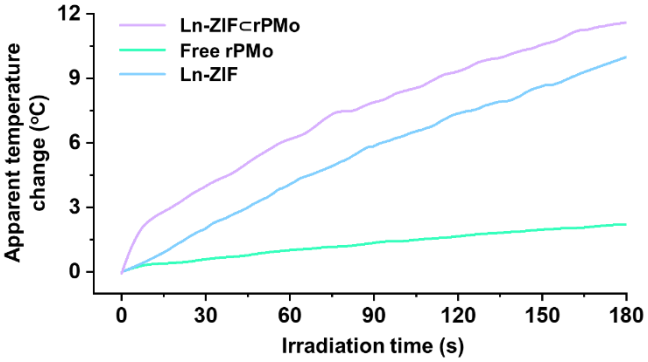

Figure S5. Photothermal effect of Ln-ZIF⊂rPMo, free rPMo, and Ln-ZIF by testing apparent temperature change recorded by a digital NIR camera. The test is performed in an aqueous dispersion under 808 nm laser irradiation at a power density of 1.25 W cm^{-2}.

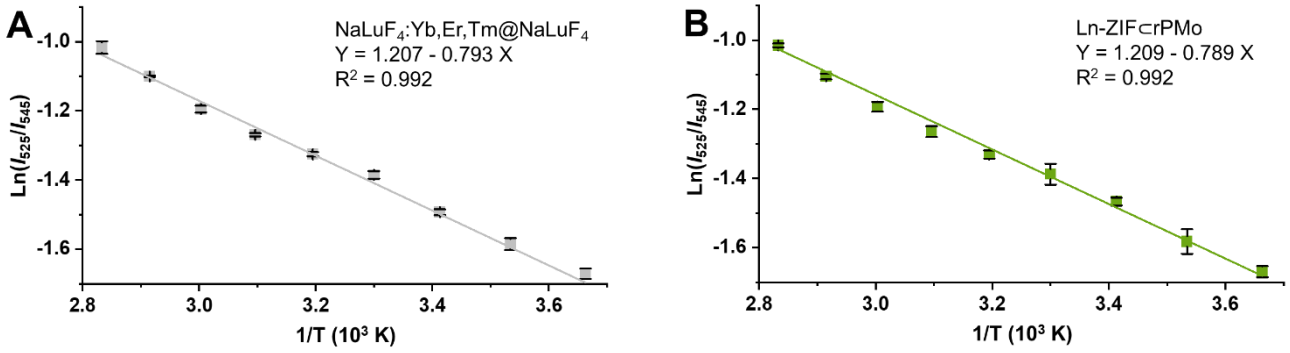

Figure S6. A plot of Ln(I_{525}/I_{545}) *vs.* 1/T to calibrate the thermometric scale for bare lanthanide nanoparticle $NaLuF_4$:Yb,Er,Tm@$NaLuF_4$ (A) and Ln-ZIF⊂rPMo (B). Data are represented as mean ± SD (n = 3).

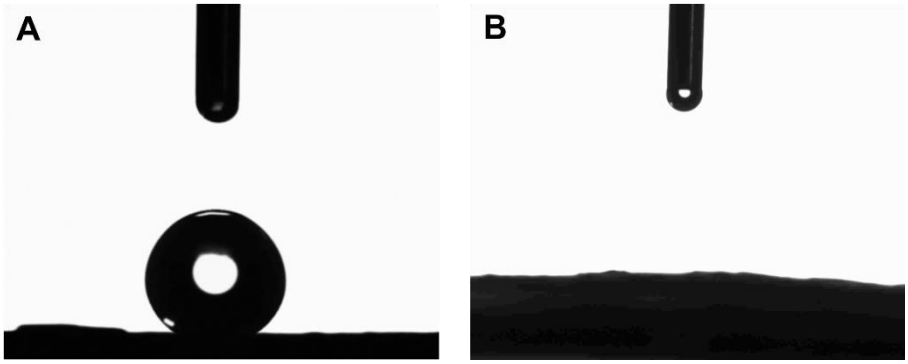

Figure S7. Water contact angle images revealed the hydrophobicity of Ln-ZIF (A) and hydrophilicity of Ln-ZIF⊂rPMo (B).

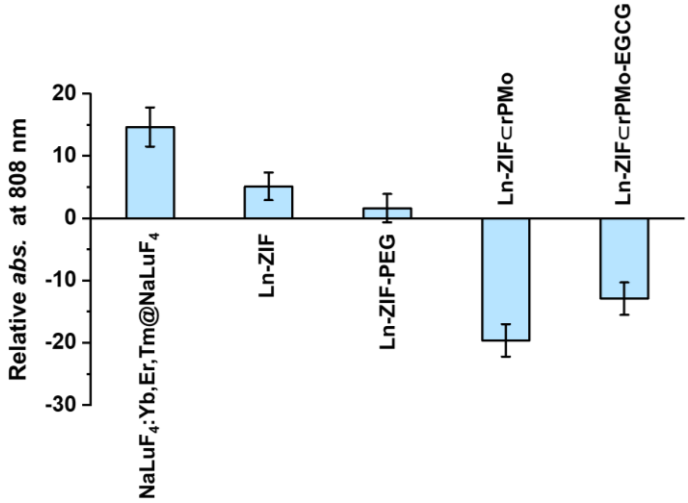

Figure S8. ζ potential of bare lanthanide nanoparticle $NaLuF_4$:Yb,Er,Tm@$NaLuF_4$, Ln-ZIF, Ln-ZIF-PEG, Ln-ZIF⊂rPMo, and Ln-ZIF⊂rPMo-EGCG. Data are represented as mean ± SD (n = 3).

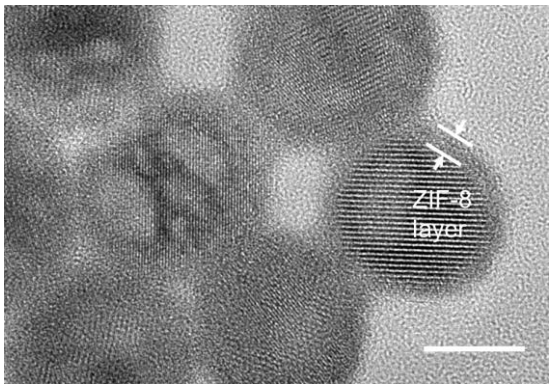

Figure S9. TEM image of Ln-ZIF. Scale bar 10 nm.

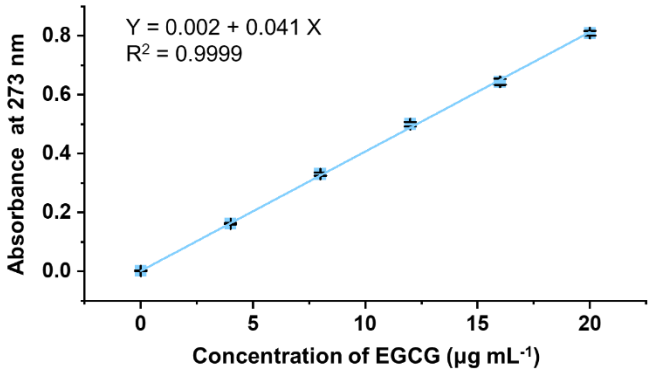

Figure S10. Linear relation between the absorbance value at the peak of 273 nm *vs.* the concentration of EGCG, which was used for quantification of EGCG loading and release. Data are represented as mean ± SD (n = 3).

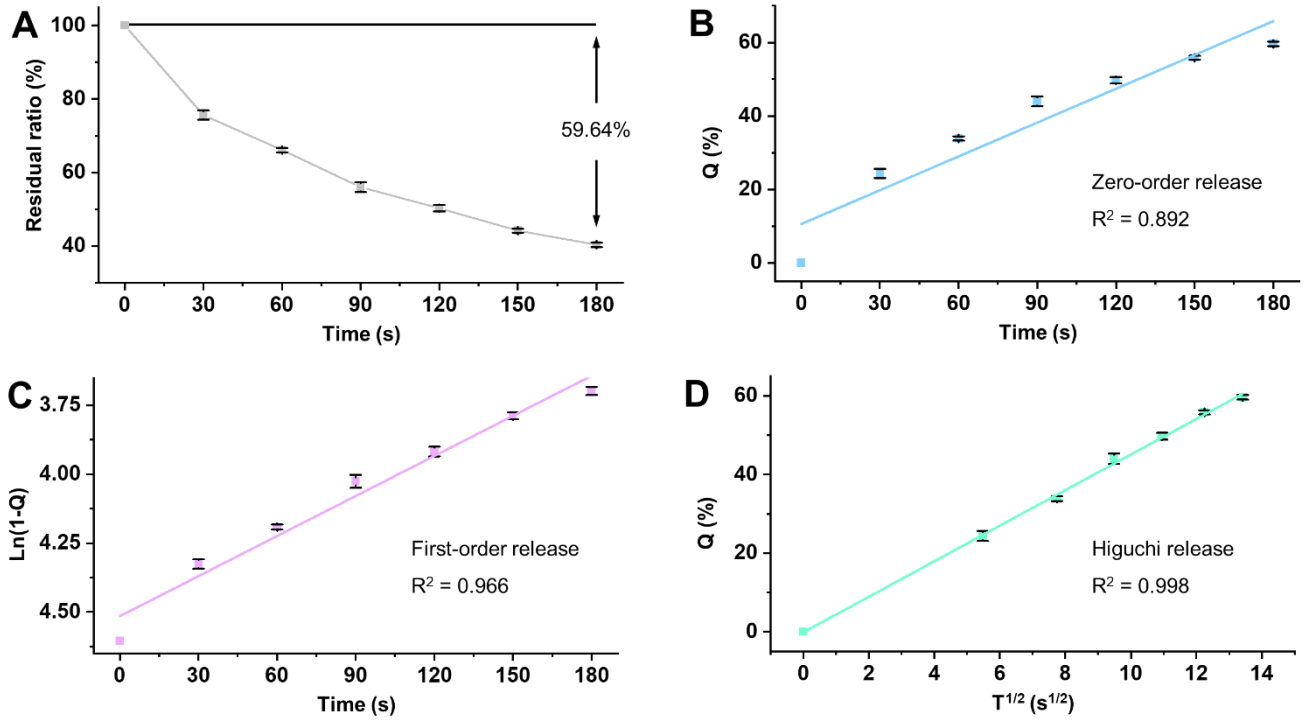

Figure S11. (A) Residual ratio of EGCG loaded on the Ln-ZIF⊂rPMo under 808 nm laser irradiation at a power density of 1.25 W cm^{-2}. The fitting curve of zero-order release (B), first-order release (C), and Higuchi release equations (D). Data are represented as mean ± SD (n = 3).

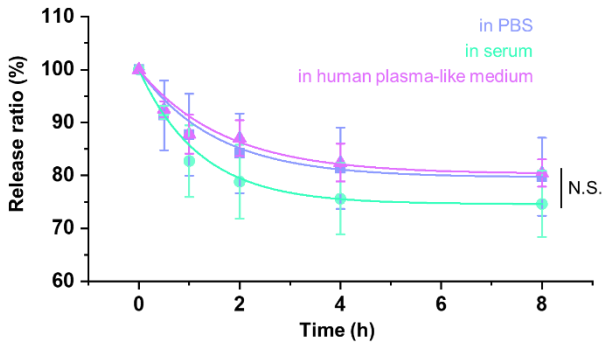

Figure S12. Temporal spontaneous release ratio of EGCG from Ln-ZIF⊂rPMo in PBS, serum, and human plasma-like medium. Statistical significance was determined by one-way t-tests. Data presented as mean ± SD (n = 3). N.S. is not significant.

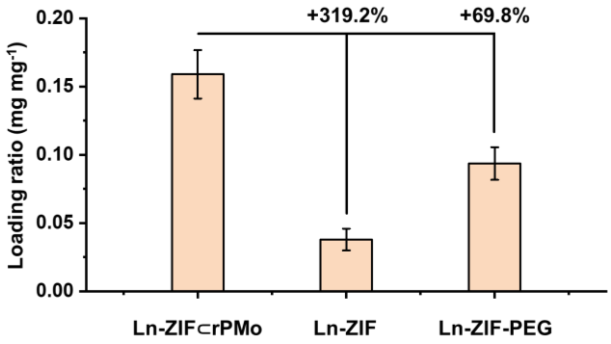

Figure S13. Loading ratio of doxorubicin hydrochloride per milligram of Ln-ZIF⊂rPMo, Ln-ZIF, and Ln-ZIF-PEG.

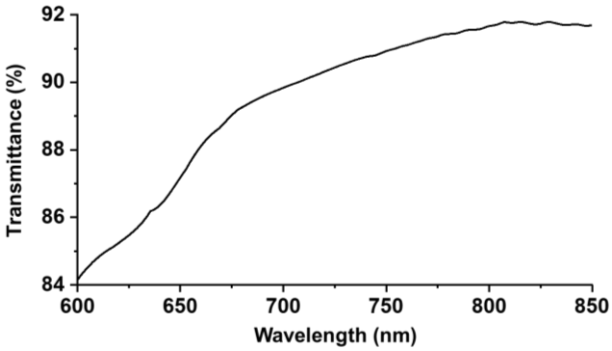

Figure S14. Transmittance of the used tissue in the red and NIR spectral range.

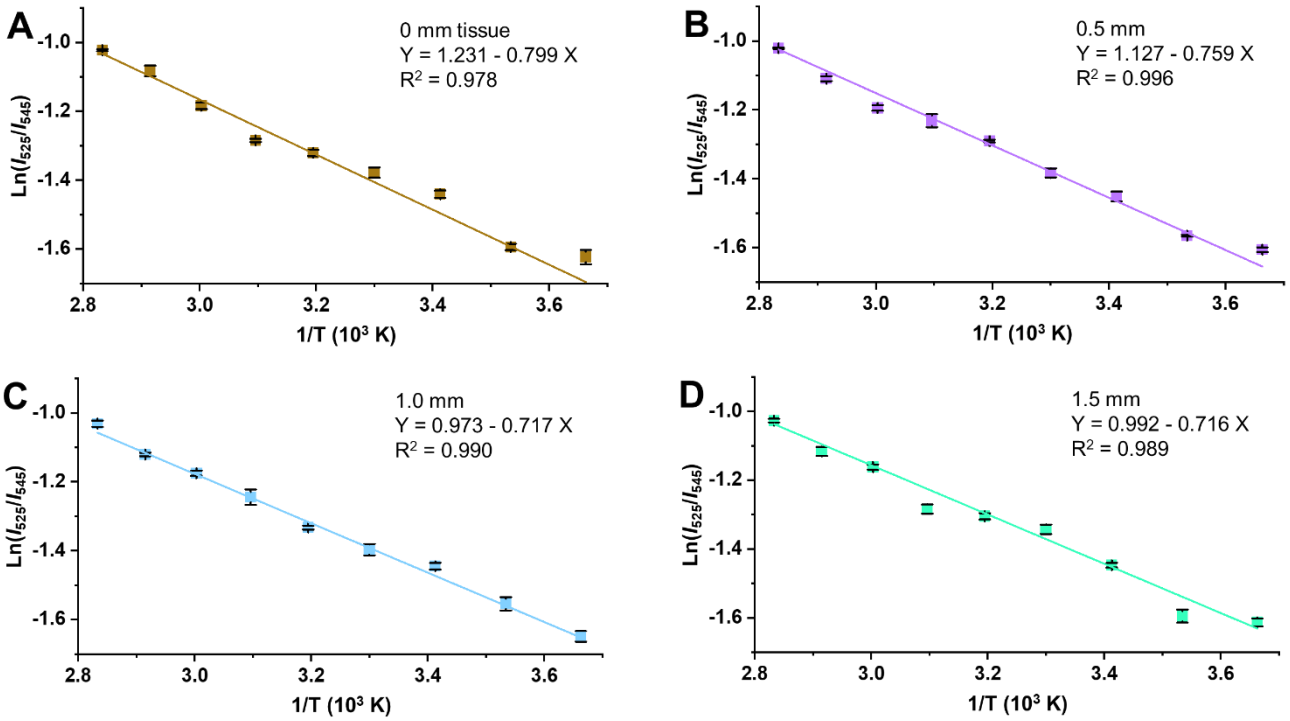

Figure S15. A plot of Ln(I_{525}/I_{545}) *vs.* 1/T to calibrate the thermometric scale for Ln-ZIF⊂rPMo-EGCG under 0 mm (A), 0.5 mm (B), 1.0 mm (C), and 1.5 mm tissue coverage (D). Data are represented as mean ± SD (n = 3).

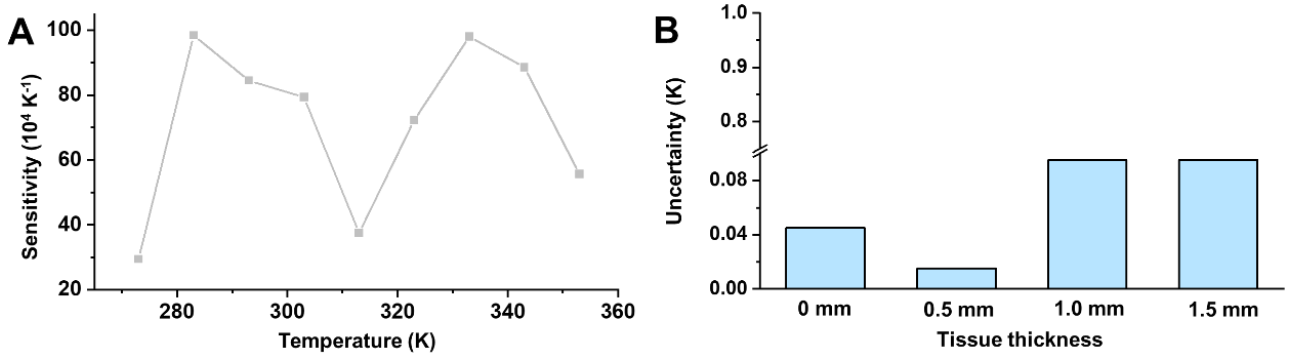

Figure S16. Thermal sensitivity (A) and temperature uncertainty (B) of Ln-ZIF⊂rPMo fluorescent nanothermometer.

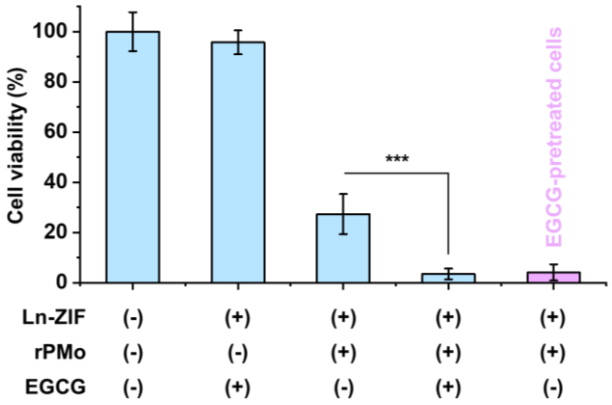

Figure S17. Cell viability of tumor cells after receiving different treatments. In the first group, the cells are only incubated with pure saline as a blank control. In the last group (pink bar), the tumor cells are pre-treated with 500 μM solution for 3 min before laser irradiation. Statistical significance was determined by one-way t-tests. Data presented as mean ± SD (n = 8). ***$p < 0.001$.

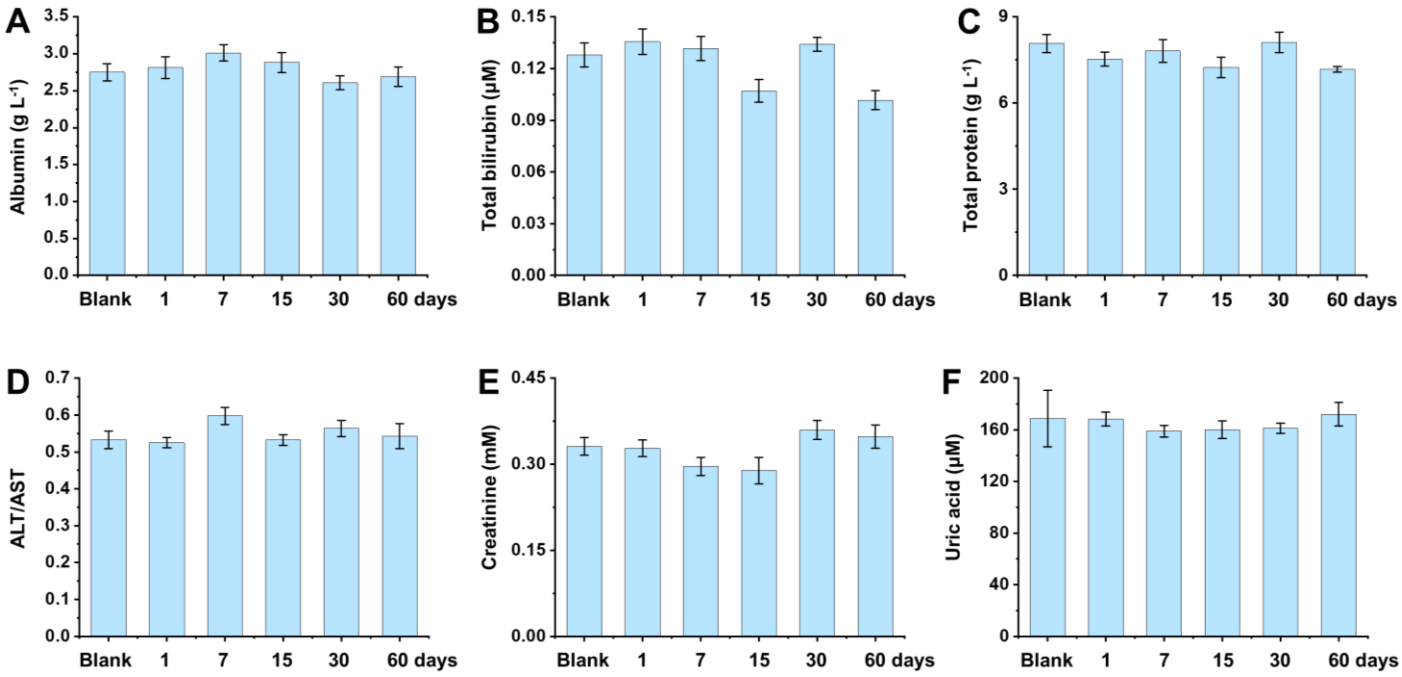

Figure S18. Serum biochemistry results, including albumin (A), total bilirubin (B), total protein (C), ALT/AST (D), creatinine (E), and uric acid (F), obtained from serum samples harvested from mice receiving Ln-mSiMo nanocomposites injection after 1, 7, 15, 30, and 60 days. ALT: alanine aminotransferase; AST: aspartate aminotransferase. Data are represented as mean ± SD (n = 3).

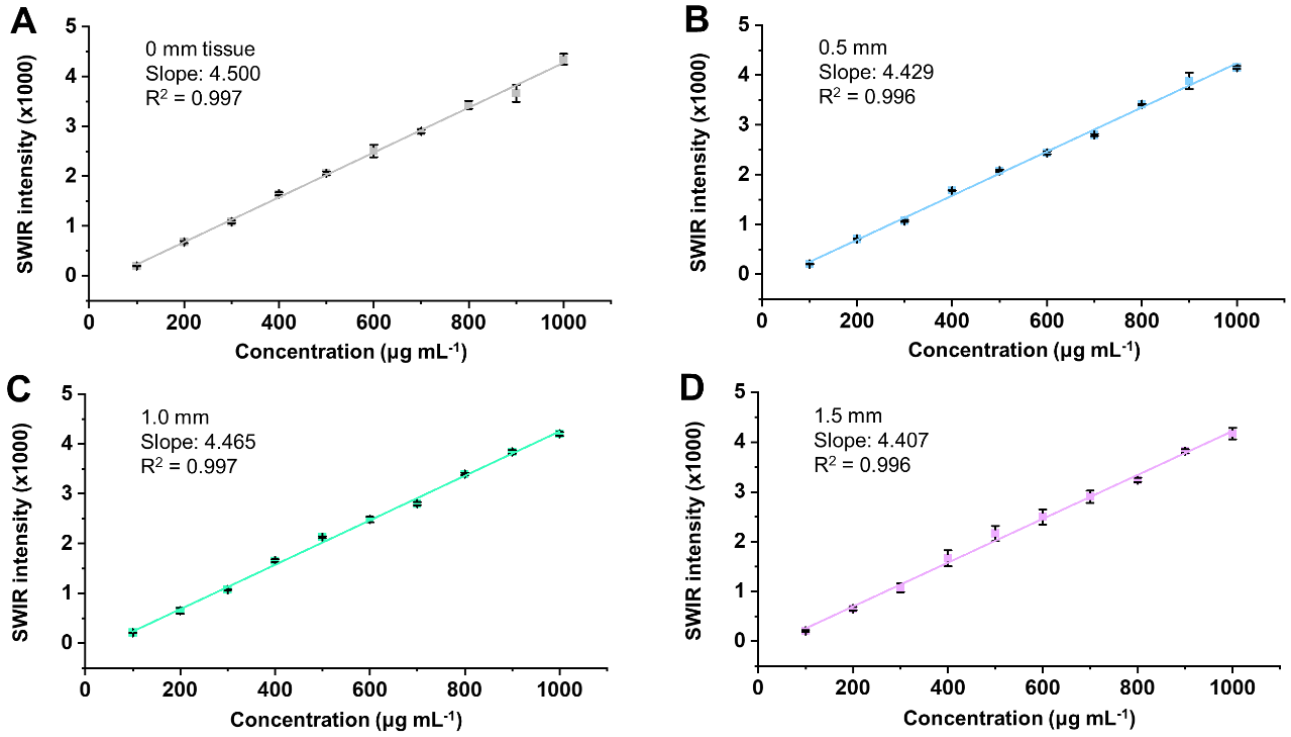

Figure S19. The relationship between the amount of Ln-ZIF⊂rPMo-EGCG and SWIR intensity under 0 mm (A), 0.5 mm (B), 1.0 mm (C), and 1.5 mm tissue coverage. Data are represented as mean ± SD (n = 3).

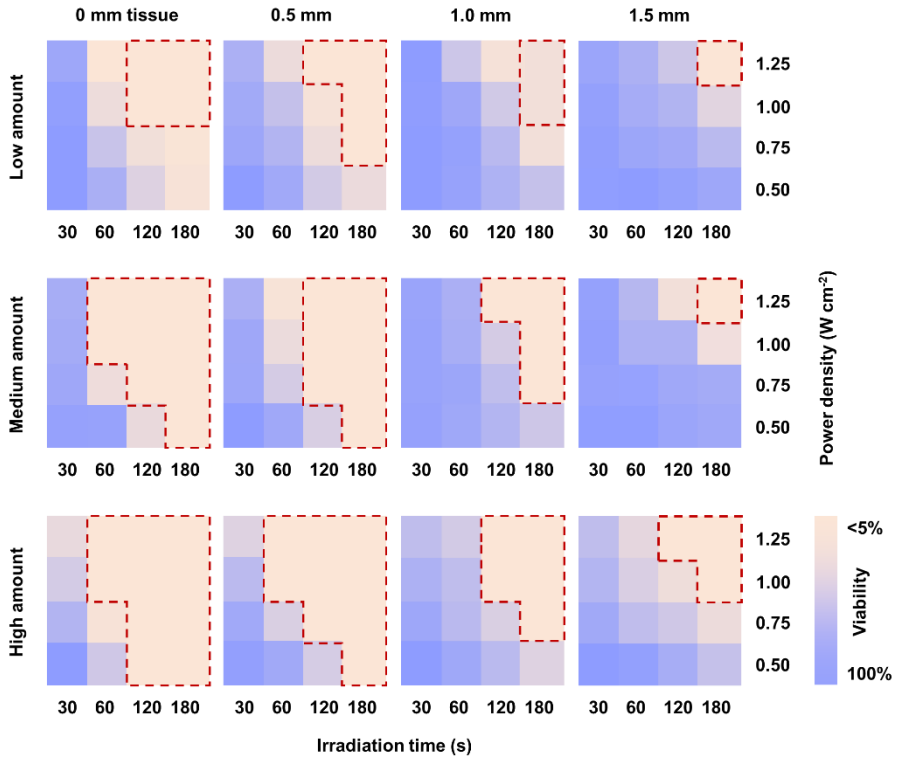

Figure S20. Viability of tumor cells incubated with Ln-ZIF⊂rPMo-EGCG under different thickness of tissue as a function of laser power density and irradiation time. Tumor cell groups with < 5% viability were highlighted.

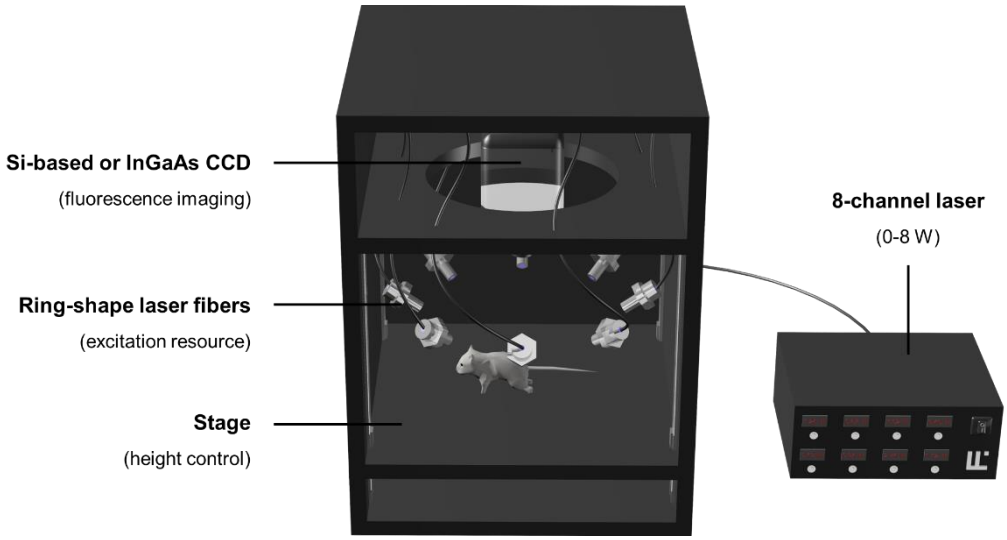

Figure S21. Brief description of the ring-shape laser array. The laser array contained 8 laser fibers that were linked to one 8-channel laser (808 nm, output power 0-8 W), which was used as the excitation source for synergistic treatment. The positions of the laser fibers were fixed (holders not shown in the image), but the angle of fibers and size of laser spots could be modulated. By adjusting the output power independently, a non-uniform light field could be generated. The power density was quantified by a power meter. The mice were fixed on the stage during the treatment, which could be adjusted in height by an internal stage. For fluorescence imaging and establishment of irradiation prescription, an Si-based (visible and NIR fluorescence) or InGaAs CCD (short-wave infrared fluorescence) was installed at the top, with one 8-channel laser (980 nm, output power 0-8 W).

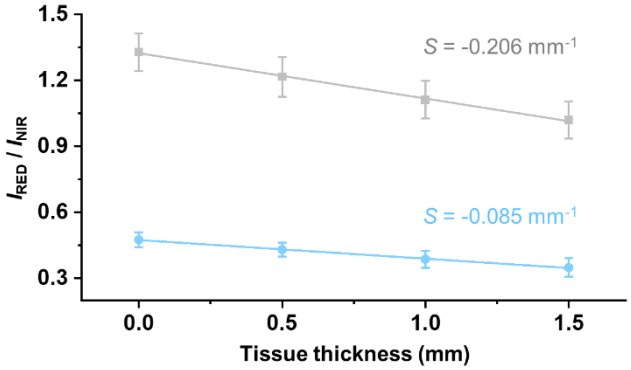

Figure S22. I_{RED}/I_{NIR} fluorescence ratio of Ln-ZIF⊂rPMo-EGCG (grey dots) and 1% Er^{3+} and 0.5% Tm^{3+}-doped $NaLuF_4$:Yb,Er,Tm@$NaLuF_4$ nanoparticle (blue dots) under different thickness of tissue. Data are represented as mean ± SD (n = 3).

Table S1. Tumor size of mice in customized irradiation group for sensitized photothermal treatment *in vivo* (unit of tumor size: mm^3).

Mouse	0.5 – 1.5 mm		0 mm	
	0 day	15 days	0 day	15 days
1	54.75	10.83	64.96	9.89
2	70.02	5.19	53.98	8.77
3	63.78	10.67	57.84	3.61
4	54.5	7.41	61.41	5.16
5	54.69	5.67	69.87	3.19
6	62.41	6.55	70.15	9.96
7	58.26	4.72	53.97	0.39
8	70.82	11.54	54.4	0.85
9	71.06	5.08	66.38	1.05
10	54.16	6.34	67.71	8.86

Table S2. Tumor size of mice in low irradiation group for sensitized photothermal treatment *in vivo* (unit of tumor size: mm^3).

Mouse	0.5 – 1.5 mm		0 mm	
	0 day	15 days	0 day	15 days
1	71.46	103.12	62.1	14.24
2	59.23	93.39	64.57	8.6
3	59.26	34.86	56.55	16.93
4	74.88	93.45	55.5	8.83
5	58.25	55.96	54.28	5.49
6	74.68	90.73	57.19	16.07
7	78.92	127.31	70.29	15.46
8	73.11	37.77	60.22	9.98
9	64.02	105.06	53.92	12.91
10	64.49	97.07	55.7	3.02

Table S3. Tumor size of mice in high irradiation group for sensitized photothermal treatment *in vivo* (unit of tumor size: mm^3).

Mouse	0.5 – 1.5 mm		0 mm	
	0 day	15 days	0 day	15 days
1	53.4	4.79	54.53	1.42
2	53.61	5.97	57.4	0.01
3	74.13	7.37	69.71	2.51
4	57.95	5.35	66.41	1.5
5	63.25	5.85	67.17	5.36
6	75.79	6.57	71.07	4.32
7	70.27	2.91	71.04	3.1
8	55.06	2.89	63.1	3.32
9	53.53	6.44	59.02	7.55
10	70.72	5.04	57.41	3.18